NASA TECHNICAL NOTE

NASA TN D-7554

NASA TN D-7554

CHARACTERISTICS AND PERFORMANCE OF SEVERAL MASS SPECTROMETER RESIDUAL GAS ANALYZERS

by William W. Hultzman

Lewis Research Center

Cleveland, Ohio 44135

NATIONAL AERONAUTICS AND SPACE ADMINISTRATION • WASHINGTON, D. C. • MARCH 1974

1. Report No. NASA TN D-7554	2. Government Accession No.	3. Recipient's Catalog No.
4. Title and Subtitle CHARACTERISTICS AND PERFORMANCE OF SEVERAL MASS SPECTROMETER RESIDUAL GAS ANALYZERS		5. Report Date MARCH 1974 6. Performing Organization Code
7. Author(s) William W. Hultzman		8. Performing Organization Report No. E-7432 10. Work Unit No. 502-04
9. Performing Organization Name and Address Lewis Research Center National Aeronautics and Space Administration Cleveland, Ohio 44135		11. Contract or Grant No. 13. Type of Report and Period Covered Technical Note
12. Sponsoring Agency Name and Address National Aeronautics and Space Administration Washington, D.C. 20546		14. Sponsoring Agency Code

15. Supplementary Notes

16. Abstract

The operation and properties of various mass-spectrometer residual gas analyzers for use in vacuum measurements were analyzed in terms of efficiencies of ion extraction, ion separation and transmission, and ion collection. Types of instruments studied were magnetic sector, omegatron, quadrupole, and monopole. Experimental results presented include absolute sensitivity to argon, relative sensitivity to 10 gases, and cracking patterns for these gases. Properties are strongly dependent on instrument range and resolution and on the particular voltages, currents, or field intensities used to control the instrument.

17. Key Words (Suggested by Author(s))	18. Distribution Statement
Mass spectroscopy Vacuum spectroscopy Gas analysis	Unclassified - unlimited Cat. 14

19. Security Classif. (of this report)	20. Security Classif. (of this page)
Unclassified	Unclassified

* For sale by the National Technical Information Service, Springfield, Virginia 22151

CHARACTERISTICS AND PERFORMANCE OF SEVERAL MASS SPECTROMETER RESIDUAL GAS ANALYZERS

by William W. Hultzman

Lewis Research Center

SUMMARY

The operation and properties of various mass-spectrometer residual gas analyzers for use in vacuum measurements were analyzed in terms of efficiencies of ion extraction, ion separation and transmission, and ion collection. Types of instruments studied were magnetic sector, omegatron, quadrupole, and monopole. Experimental results presented include absolute sensitivity to argon, relative sensitivity to 10 gases, and cracking patterns for these gases. Properties are strongly dependent on instrument range and resolution and on the particular voltages, currents, or field intensities used to control the instrument.

INTRODUCTION

In many high vacuum applications, it is important to identify the gas species present as well as to know the approximate pressure level. Examples where such information is useful are materials research, spacecraft and space power system tests, thin-film processing, and outgassing, gettering, and pumping studies. Such measurements are commonly made with mass-spectrometer residual gas analyzers (hereafter termed RGA's). Descriptions of RGA's in current use are given in references 1 to 11. To determine pressures and identities of individual gases, knowledge of three major RGA characteristics is required. These are absolute sensitivity to a reference gas, relative sensitivity to other gases, and the cracking pattern of the measured gases. The cracking pattern denotes the total spectrum of ions that appear when a particular gas is ionized, expressed as percentages of the principal ion. The cracking phenomenon results from the presence of isotopes and from the processes of dissociation and single and multiple ionizations. Absolute sensitivity, as used in this report, is the ratio of indicated output current contributed by either the principal ion, or the sum of all ions in the

gas cracking pattern, to the partial pressure of the gas (amperes/torr).

Relative sensitivity is the ratio of absolute sensitivity for a particular gas to that for a standard gas, such as nitrogen or argon. Argon was used in the present work.

For total-pressure measurements made with ionization gages, relative sensitivity is substantially invariant with gage type and closely correlated with gas ionization cross section (refs. 12 and 13). However, for RGA's, relative sensitivity also depends on efficiencies of ion separation and collection. These properties are unique to individual RGA design and operating parameters.

Much information is available on absolute and relative gas sensitivity as a function of upstream or sample reservoir pressure in analytical chemistry applications. However, it is difficult to use this information to measure absolute partial pressures in a vacuum environment unless flow characteristics of both the gas inlet and vacuum system under consideration are accurately known. Only a limited amount of information exists in the literature on RGA relative sensitivities for partial-pressure measurement. This is especially true for the intercomparison of different types of RGA's on the same vacuum system.

This investigation was primarily concerned with determining sensitivities and cracking patterns of several types of RGA's in common use at the Lewis Research Center. Instruments studied and intercompared included three magnetic sector types, a quadrupole, a monopole, and an omegatron. Only commercially available instruments were studied. The tests were performed with 10 different gases at a pressure level of about 2×10^{-7} torr.

The first part of this report is tutorial. It describes the basic characteristics of the types of RGA's which were evaluated and is meant to aid a potential user in selecting a RGA for a particular application.

Symbols used are listed in the appendix.

CHARACTERISTICS OF RESIDUAL GAS ANALYZERS

A typical RGA normally consists of the three regions shown in figure 1: a source region in which the gas molecules are ionized, a separator region in which ions of different values of mass-to-charge ratio m/q are separated, and a collector region where ions of a specific value of m/q are collected. In the RGA, all of these regions are nominally at the same pressure.

In the first region, the ion source and accelerator, an electron current i^- is caused to travel over a path length ℓ. The total number of ions created by electron bombardment of gas molecules is equal to $n\sigma\ell i^-$ where n is the molecular density and σ is the total ionization cross section. The extraction of ions of a particular

value of m/q through the exit aperture of the first region is performed with an efficiency β, which depends on exit-slit dimensions, operating potentials, magnetic field intensities, and the value of m/q.

In the second region only a fraction of ions that are extracted from the source pass through the entrance aperture or slit of the detector. This fraction is denoted by τ, the transmission efficiency. Its value depends on the separating principle used, the electric and magnetic potentials used in the separator, the absolute pressure, and the value of m/q. In this investigation it was not possible to separate τ from β; hence, the product $\beta\tau$ will be designated by the symbol η, termed the efficiency.

If the third region is a Faraday-cup ion detector, all ions entering the entrance slit will be collected and measured as a current numerically equal to the entering ion current. If the detector is an electron multiplier, the ratio of output current to entering ion current can be represented by a gain A. The value of A is a function of m/q, ion energy, ion molecular structure, and the operating parameters of the electron-multiplier structure.

The three regions enumerated will be treated in greater detail in the next sections.

Ion Source and Accelerator

In the ion source region the dissociation of the gas molecules is produced by electron bombardment and by contact with electrode surfaces. New compounds may also be formed by surface reactions with incident ions or molecules; these compounds may also become ionized. All of these ions, including those resulting from isotopes, may produce an elaborate cracking pattern when a single gas species is ionized.

The total ionization cross section σ, as ordinarily published (ref. 14), is usually sufficient to give a close approximation to the number of ions created. Table I lists the total ionization cross section of the gases used in the present tests at three different electron energies, 75, 100, and 150 electron volts. In the instruments investigated, the electron energy lay within this range of values. The total cross section σ, based on an average electron energy of 100 electron volts, is used later in this report to calculate both relative and absolute ion collection efficiencies for the various RGA's.

The extraction efficiency β varies with m/q and is influenced by the following factors, which also affect cracking patterns and ion trajectories (refs. 15 and 16):

(a) Ion beam thermal energy distribution

(b) Electron beam current

(c) Electron beam shape

(d) Electron beam focusing magnetic field intensity

(e) Space charge effects

(f) Surface charge effects

(g) Ion repeller potential (refs. 17 to 19)

(h) Kinetic energy of created ions

(i) Penetration of ion accelerating voltage into ionization region

(j) Stability of voltage supplies

(j) Exit slit dimensions.

Two designs of ion source and accelerator are shown in figure 2. In figure 2(a) the electron path is in the same direction as the emergent ion beam. In figure 2(b), the more common arrangement, the electron beam is at right angles to the ion beam, and a repeller electrode is normally used to direct the ions into the acceleration region. In both of these cases axial electric fields are used to draw out the ions from the ionizing region and to accelerate them. On leaving the grounded collimating slit, acceleration ceases, and thereafter the ions move at a constant axial velocity that depends on their mass-to-charge ratio and initial accelerating voltage.

Neither of these designs is representative of the omegatron ion source, which must be considered implicitly with the m/q separator mechanism.

Mass-to-Charge-Ratio Separator

Principal performance characteristics of the m/q separator are the transmission efficiency τ and resolving power or resolution. Although there are many ways of specifying resolution (ref. 20), the definition used in this report is the value $M_s/\Delta M$, where M_s is the specific atomic mass in specific atomic mass units (samu), and ΔM is the width of the peak (in samu) measured at 1 percent of peak height. The specific atomic mass M_s is the atomic mass M (in amu), divided by z, the number of charges removed from the particle. For single ionization, which is the most common process, $M_s = M$.

The absolute mass m is also frequently used in this report. It is related to M by $m = M/N_A = 1.66053 \times 10^{-27}$ M kilograms, where N_A is the Avogadro number.

Figures 3 to 5 show the four basic designs of separators studied in this experiment.

Sector. - Figure 3(a) shows the basic principle of the magnetic sector design. Normally, the source exit slit, the collector entrance slit, and the vertex of the magnetic sector are colinear. When magnetic field fringe effects are neglected, the condition that the two slits be confocal is

$$\frac{m}{q} = \frac{1}{2} R^2 \frac{B^2}{V} = \frac{1}{8} L^2 \frac{B^2}{V} \sin^2 \frac{\theta}{2}$$

where V is the voltage used to accelerate ions that leave the ion source and B is the magnetic flux density of the sector field. Scanning (sequential focussing of desired ions) may be performed either by varying the accelerating voltage (V-scanning) or by varying the magnetic field (B-scanning).

The size of a sector RGA is often expressed in terms of the ion-beam radius of curvature R because both resolution $M_s/\Delta M$ and dispersion D (the transverse separation at the collector slit of particles differing by one amu) are proportional to R. These quantities are related by

$$D\frac{M_s}{\Delta M} = R = \frac{L}{2}\sin\frac{\theta}{2}$$

Increasing L (and R) reduces the fringe effect of the magnet on the source and collector because separation is increased. However, the improvement in resolution is mitigated by an increase in beam broadening and aberration effects. These effects are caused by fluctuations in accelerating voltage V, variations in the angle at which the beam leaves the ion source, and space charge effects. The effect of these aberrations is reduced as collector slit width is reduced but this reduction also decreases the sensitivity.

Therefore, R, θ, and the slit widths must be chosen to effect an optimum balance between sensitivity s, resolution $M_s/\Delta M$, and efficiency τ (ref. 17).

For sector instruments, resolution $M_s/\Delta M$ is essentially independent of mass.

Omegatron. - Figure 3(b) illustrates the basic principle of the omegatron. The ionizing electron beam is focused by and is parallel to the magnetic field B. A transverse alternating electric field produces a spiral ion trajectory. Only ions satisfying the governing equation

$$\frac{m}{q} = \frac{B}{\omega_c}$$

(where the quantity ω_c is the cyclotron frequency and is also the frequency of the alternating electric field) will receive sufficient energy to reach the collector.

By analogy with the sector type of instrument, ions are extracted from the region of the electron beam, with an extraction efficiency β. The value of β is influenced by the trap voltage, by radio-frequency (rf) voltage amplitude V_{rf}, and by electron and ion beam intensities (ref. 21).

Transmission efficiency τ is affected by ion scattering and by drift to other electrodes along the spiral trajectory of resonant ions to the collector. The resolution is given by

$$\frac{M_s}{\Delta M} = \frac{r_o B^2}{V_{rf} M_s}$$

where r_o is the radial distance from the electron beam to the ion collector (ref. 22).

Quadrupole. - The quadrupole instrument separates ions solely by electric fields. Four cylindrical electrodes (preferably hyperbolic but usually circular in cross section) are used. The cylinders are mounted precisely at the corners of a square; diagonally opposite rods are separated by a distance of 2r (as shown in fig. 4(a)). Cylinder radius is normally 1.16 r to approximate the hyperbolic field. The pair of cylinders in the xz plane is energized with a potential of the form $U + V_{rf} \cos \omega t$. The electrodes in the yz plane are at a potential $-U - V_{rf} \cos \omega t$. The frequency ω is in the rf range. The field configuration is indicated in figure 5(a).

Ions injected along the centerline of the array travel along paths resembling those shown in figure 4(b) with maximum amplitude dependent on entrance angle (ref. 23). Ion trajectories are usually described in terms of Mathieu differential equations containing dimensionless parameters a and q', values of which define the stability limits for the injected ions (ref. 9). The values of a and q' are given by

$$a = \frac{8U}{r^2 \omega^2} \frac{q}{m}$$

and

$$q' = \frac{4V_{rf}}{r^2 \omega^2} \frac{q}{m}$$

The stability diagram is shown in figure 5(b). Only ions with values of m/q, such that a and q' fall in the stable (cross-hatched) area of the stability diagram will traverse the full length of the rods and be collected. All other particles will collide with one of the four electrodes.

Scanning, or ion selection, is usually accomplished by holding U/V_{rf} almost constant (ref. 24), while varying the amplitude of U and V_{rf} along an operating line, as shown. Resolution, which is proportional to U/V_{rf}, is a maximum, but ion collection is a minimum, when the operating line has a slope of 0.336 and just passes through the apex of the diagram.

If scanning is accomplished by varying voltage amplitude (while keeping U/V_{rf} constant), dispersion remains constant, resulting in a linear spacing between adjacent

mass peaks when these are plotted as a function of V_{rf}. Since peak width is constant, resolution increases directly with M_s. If scanning is accomplished by varying frequency, dispersion is nonlinear and resolution $M_s/\Delta M$ remains constant as in sector instruments.

The unique capability of the quadrupole RGA lies in the operator's ability to control resolution by changing the ratio U/V_{rf}. In a sector RGA, resolution depends primarily on source- and exit-slit widths and on ion-path radius R; these normally cannot be altered. In both sector and quadrupole RGA's, efficiency τ varies inversely with resolution. In the case of the quadrupole RGA, the closer the operating line $2U/V_{rf}$ = constant is to the tip of the shaded area (fig. 5(b)), the greater is the resolution. However, resolution is also affected by ω (ref. 25) and by voltage supply stabilities, precision of mechanical dimensions, and ion beam energy. Fringing fields between the rods and the entrance and exit apertures adversely affect transmission of the heavier ions (ref. 23).

Monopole. - The monopole separator is a simplification of the quadrupole design, based on the fact that the planes represented by lines A-A in figure 5(a) are at ground potential. The monopole separator (fig. 4(c)) therefore uses a single rod and a V-shaped grounded trough as the two electrodes. The length of the electrodes must be less than the length L' shown in figure 4(b) so that stable ions may be collected by the detector before they collide with the grounded electrode. As can be seen from the shape of the cross-hatched portion of the stability diagram of figure 5(b), resolution is almost independent of the ratio U/V_{rf} over fairly wide limits of this ratio. Power supply stability requirements are therefore less severe than for the quadrupole. Resolution is controllable only to a limited extent by changing the energy of the injected ions.

Ion Detector

Unity-gain detector. - This detector may be as simple as a single metallic electrode, as used in the omegatron, or it may be in the form of a Faraday cup, designed to collect all the ions passing through the entrance slit and to suppress loss of charges through secondary emission. Since the output current is equal to the incident ion current (A = 1), a long time-constant electrometer circuit is necessary to accurately measure the minute current. In contrast to the electron-multiplier detector, gain is not affected by pressure level or by the nature of the gas and is unchanged by previous exposure of the detector to air.

High-gain detector. - An electron multiplier may be used to provide a high ratio between output current and detected ion current, and to provide fast response and

short spectrum scan time. A current gain A of 10^6 is typical. Disadvantages are that gain is dependent on gas species, ion energy (ref. 26), pressure level, and history of exposure to air and other gases (ref. 27). This last effect may cause the gain to drift with time. Gain may also be affected by ambient magnetic fields. This characteristic is particularly objectionable when the magnetic field varies (such as in B-scanning by a sector instrument). Magnetic shielding is usually provided in such applications to minimize possible effects.

TEST EQUIPMENT AND TESTS

Performance Characteristics Determined

The characteristics of the instruments tested are listed in table II. For each instrument (except the $90^\circ/135^\circ$ sector instrument), the following performance parameters were determined:

(1) s_{Ar}, absolute sensitivity to argon

(2) s_G/s_{Ar}, relative sensitivity, for all or most of the following gases: hydrogen, helium, neon, nitrogen, carbon monoxide, oxygen, carbon dioxide, krypton, and xenon

(3) δs_{Ar}, stability of sensitivity to argon

(4) η_G/η_{Ar}, relative efficiency (for instruments with unity-gain dectors)

(5) $(\eta A)_G/(\eta A)_{Ar}$, relative product of efficiency and gain (for instruments with electron multipliers)

(6) Cracking patterns for the various gases.

Only cracking patterns were recorded for the $90^\circ/135^\circ$ instrument because it was not located in the calibration chamber. To cover the complete mass range for this instrument, two separate ion collectors are provided. One converts the RGA into a 135° sector (1 to 10 samu), and the other into a 90° sector (10 to 80 samu).

Sensitivities are expressed as output current divided by partial pressure. Generally, two ways were used to define the output current: the height of the principal ion peak and the sum of the heights of all peaks generated in the cracking pattern.

Calibration System

The calibration system and calibration method are illustrated in figure 6. The conductance pressure divider principle (refs. 28 and 29) is used for RGA calibration. A tandem arrangement of three chambers is evacuated by a triode ion pump having a

speed of 1000 liters per second for nitrogen and 300 liters per second for argon. Preliminary evacuation is performed with a 10-centimeter pumping station, consisting of a liquid-nitrogen cold trap, a DC 705 oil diffusion pump, and a mechanical pump.

Successive chamber volumes are about 3, 23, and 28 liters. Chambers are separated by circular orifices cut into 25-micrometer-thick stainless-steel sheet. The upper and lower orifices are about 1 millimeter and 32 millimeter in diameter, respectively, with nitrogen conductances of about 0.09 and 96 liters per second, respectively.

Identical model Bayard-Alpert ionization gages are mounted on the lower two chambers and a high-pressure ionization gage is mounted on the first chamber. The RGA's to be calibrated are mounted on the second chamber coplanar with the Bayard-Alpert gages. One RGA, the $90^{\circ}/135^{\circ}$ sector type, is mounted on chamber 3. Test gases are admitted into chamber 1 so that there is continuous stable flow through the system. Typical operating pressures are 2×10^{-4} torr in the upper chamber, 2×10^{-7} torr in calibration chamber 2, and a decade lower in chamber 3.

The entire assembly is bakeable at 400° C. Ultimate pressure of the baked-out system is about 6×10^{-10} torr, with all instruments operating.

Calibration Method

The calibration method consists of establishing a known steady calibration-gas influx Q through a calibrated leak with an accurately measured inlet pressure p_0 of about 800 torr. For molecular flow

$$Q = G_{23}(p_2 - p_3) \tag{1}$$

where G_{23} is the conductance of the lower orifice computed from an accurate measurement of its diameter (Clausing's (see ref. 30) and Bureau's et al. (ref. 31) corrections were negligible), and p_2, p_3 are the respective pressures in chambers 2 and 3 corrected for initial background pressures. Equation (1) may be written as

$$p_2 = \frac{Q}{G_{23}} \frac{1}{1 - \frac{p_3}{p_2}} \tag{2}$$

It is assumed that the ratio

$$\frac{p_3}{p_2} = \frac{i_3^+}{i_2^+} \frac{S_3}{S_2}$$

where i_2^+ and i_3^+ are the respective ion-collector currents, due to the calibration gas, of gages PG2 and PG3 and S_2 and S_3 are their respective sensitivities. Both gages are subjected to the same gas during RGA calibration, and both are of the same model. The sensitivities of these gages had previously been determined by Holanda using the apparatus described in reference 32. Because the ratio p_3/p_2 is in the range of 0.05 to 0.42, depending on gas pumping speed, a 10 percent uncertainty in estimating the ratio S_3/S_2 yields a 0.5- to 7-percent uncertainty in p_2.

The estimated maximum inaccuracy in p_2 for the results reported herein is in the range 2 to 8 percent, depending on the gas being measured.

Since $p_0 \gg p_1$, throughput Q for the calibrated leak is given with adequate accuracy by

$$Q = G_0 p_0 \tag{3}$$

where G_0 is the independently determined conductance of the leak. The maximum inaccuracy in G_0 is 1 percent.

Auxiliary Apparatus and Measurements

Figure 7 shows the piping arrangement of apparatus used to calibrate the leak and to make some other measurements of incidental interest. The normal flow of gas is through valves V8, V6, and V1. The calibrated leak is a cylindrical plug of sintered platinum, 4.8 millimeters in diameter and 1.2 millimeters thick, and is mounted in a compression type of tube fitting. Its conductance for argon with atmospheric pressure upstream is about 2×10^{-8} liter per second; the flow is in the molecular-flow regime. Upstream pressure at the leak is measured by a quartz bourdon-tube differential manometer connected through valves V10 and V6. The reference side of the manometer is connected through valve V11 (with V9 closed) to the vacuum created by the mechanical pump. Valve V1 is open during RGA calibration and closed during leak calibration. Valve V12 is opened only to clean up the inlet system after runs.

To calibrate the leak, a 0- to 1-torr capacitance-type diaphragm manometer is connected to the downstream side of the leak through valve V4. The reference side of this manometer is connected to substantially-zero pressure p_2 through valve V7 (V5 is closed). An additional calibration volume V_c is attached to the downstream side

of the leak through valve V3. Pressure p_0 of the gas upstream of the leak to valve V6 is set to exactly 800 torr by adjusting variable leak V8. Valve V8 is then closed; the trapped volume is sufficiently large so that p_0 thereafter does not deviate more than 0.1 percent from 800 torr during the course of the subsequent calibration. With valves V1, V2, and V5 closed the volume V_d of the entire system downstream of the leak previously determined, the rate of rise of pressure p, indicated by the diaphragm manometer when valve V6 is opened, is noted. Volume V_d includes both the volume of the system shown by the heavy lines and the volume V_c of the calibration volume (V3 is open).

Inasmuch as p_0 is much greater than the maximum value of p (800 torr versus 0.9 torr), after a short time lag t_a (about 0.3 min) to allow for surface adsorption and system time constant, gas flow is uniform and dp/dt is constant. Since

$$\frac{dp}{dt} = \frac{G_0}{V_d} p_0 \tag{4}$$

for $t > t_a$ and $p_0 \gg p$, the conductance G_0 can be calculated.

Separate determination of volume V_d was made, through use of Boyle's Law, by

(1) Creating a pressure of 1 torr in V_d, as measured by the capacitance manometer, then closing V3 to trap this pressure in V_c

(2) Evacuating the remainder of V_d by opening V2

(3) Closing V2, then opening V3 and observing the new pressure indication. Short term leakage through the porous leak is negligible.

The ratio of the two pressures indicated by the capacitance manometer is equal to V_d/V_c. Volume V_c was separately determined by filling it with mercury and weighing. Volumes V_c and V_d were about 6 and 30 cubic centimeters, respectively.

Valves V5 and V9 are used to set zero on the manometers. Other valves are used to permit cleaning the system by evacuation with one of the vacuum pumps. The diaphragm manometer may also be used to monitor the pressure difference $p_1 - p_2$, through valves V2 and V7, during an RGA calibration.

From equations (2) to (4), the final equation for calibration-gas pressure is

$$p_2 = \frac{V_d}{G_{23}} \frac{dp}{dt} \frac{1}{1 - \frac{p_3}{p_2}} \tag{5}$$

Calibration Procedure

The sequence of the normal calibration procedure was as follows: After the system had been at an ultimate pressure of about 6×10^{-10} torr for several hours, test gas inlet pressure p_0 was adjusted to 800 torr. After 1 to 2 hours, during which, presumably, surfaces became saturated with the test gas, pressure p_2 in the test chamber stabilized at 1×10^{-7} to 3×10^{-7} torr. Readings of the RGA's and ion gages could then be made.

In order to determine the ratio i_3^+ / i_2^+ of the ion gages with maximum accuracy, the same gage control unit was used for both gages. However, while the gage being read was connected to this control unit, the other gage was connected to a second control unit so that electrode and gage temperatures remained substantially unchanged. The roles of the two control units were interchanged when the second gage was being read. A stabilizing period of about 5 minutes was required after switching control units.

Each RGA was tuned to maximum sensitivity for argon on the most useful range of that instrument (see table II). The tuning was not changed thereafter regardless of test gas or instrument range used. Where applicable, operating currents and voltages were those recommended by the manufacturer (these are shown in table II). However, since a calibration with argon and the test gas were always performed on the same day, the tuning was a daily occurrence.

In the case of the quadrupole RGA, the resolution control was adjusted for a ΔM of one specific atomic mass unit for both ranges listed in table II.

A calibration run involved manually scanning and recording all the peaks of the cracking pattern of the test gas for each RGA as well as recording the ion gage readings. An average run for one RGA took 10 to 15 minutes. Since some of the RGA's had two ranges, total duration of the calibration was 2 to 3 hours.

Immediately after the calibration for each gas, the calibrated-leak conductance G_0 was measured while the test gas or argon was still connected. Time of leak calibration was about 10 minutes. The rate of pressure rise dp/dt was such that final diaphragm-manometer pressure was 0.2 to 0.9 torr, depending on the test gas. The drift of the value of G_0 for argon over a period of 120 days is shown in figure 8. The drift is believed to be due to gradual clogging of the porous material. The effect of room temperature fluctuations on the leak was negligible.

Because of the "memory effect" of the ion pump, (re-emission of previously pumped gases), traces of the test gas were evident to some extent when argon was measured. Such residual effects were more prominent when the test gas was inert. Therefore, the test gas was always measured first on the daily runs. Also, when the test gas was

neon, nitrogen rather than argon was used as the reference gas, to minimize the interference of $^{40}Ar^{++}$ with $^{20}Ne^{+}$, and any necessary correction was made.

The data presented generally represent the averages of three runs for each test gas and for argon.

RESULTS AND DISCUSSION

Absolute Sensitivity to Argon

Effect of history. - Figure 9 presents the value of s_{Ar} for the various RGA's, measured on the same day that the value of s_G was determined. There are no data when neon was the test gas, because nitrogen, rather than argon, was used as the reference gas. This procedure was necessary because of the residual effects mentioned earlier.

In the case of the monopole RGA, there was a shift in sensitivity when the instrument was retuned after run 6. Monopole RGA sensitivity was very sensitive to tuning adjustments.

Effect of range setting. - The sensitivity of the same instrument on different ranges may vary considerably (as indicated in fig. 9). For the 60° sector RGA, high-range A2 provides nearly an eightfold higher sensitivity over the low-range A1. The difference is due principally to the change in accelerating voltage V and its effect on the extraction of ions from the ion source, that is, on the value of extraction efficiency β (ref. 33). A similar effect on β in the case of the 90° sector RGA (B-1 and B-2) was masked by the detuning caused by the shift to magnetic scan. (Peaking was performed on the B-1 or voltage scan mode). In the case of the quadrupole RGA (E-1 and E-2), the transmission efficiency τ was decreased by a factor greater than 3 when the frequency was reduced to cover the high range (ref. 25). For the monopole RGA, argon sensitivity on the high range F-2 was over four times higher than that of the low range as a result of decreasing the ratio U/V_{rf} to cover the high mass range. The resolution decreased in about the same proportion.

Effect of exposure to oxygen. - Almost all instruments showed noticeable effects of prolonged exposure to oxygen, as can be seen after run 20 (fig. 9). These effects were not consistent among different instruments, but were similar for both ranges of the same instrument. Both ranges of the 60° sector RGA showed a pronounced rise in sensitivity, but recovered after an elapsed time of almost 3 months. The omegatron and monopole RGA's (also with Faraday cup detectors) did not show the same type of change as the 60° sector RGA. As shown by figure 9(b), both ranges of the 90° sector RGA showed a pronounced drop, but no recovery, while the quadrupole RGA (E-1 and

E-2) showed a modest change. Although the 90° sector RGA and the quadrupole RGA both had electron multipliers, they used different dynode materials.

Long-term average sensitivity. - The average value of s_{Ar} and its average deviation based on 17 calibrations (runs 1 to 20, fig. 9) before exposure to oxygen are shown in table III. On the average, s_{Ar} varies about 12 percent. The shift in s_{Ar} on exposure to oxygen varies from a 1.3-fold decrease to a 3-fold increase among different RGA's (fig. 9).

Relative Sensitivities and Efficiencies

Value of relative sensitivity s_G/s_{Ar}. - Tables IV and V list s_G/s_{Ar}. Table IV lists relative sensitivities based on principal peak only, and table V gives relative sensitivities based on the sum of all peaks of the cracking pattern. The numerical values in the two tables are alike within 20 percent in 90 percent of the entries, if the krypton and xenon data are excluded.

Relative sensitivity may be a strong function of resolution. Values of s_G/s_{Ar} for gases with many isotopes of significant magnitude, such as krypton and xenon, are particularly sensitive to the resolution, because of cross-contribution of isotope peaks. Figure 10 illustrates how the resolution setting of an E-1 quadrupole affects its measurement of the background pressure of a diffusion-pumped vacuum system. Relative sensitivity in this figure is given with respect to hydrogen because the dependence of τ on resolution is a stronger function of resolution for ions with large m/q ratios than for lighter ions. This effect can be minimized by designing the electronic circuit so that there is a proper automatic variation of the ratio U/V_{rf} during mass scanning (ref. 34).

Value of relative product of efficiency and gain $(\eta A)_G/(\eta A)_{Ar}$. - Table VI presents the numerical data of table V after division by the ratio σ_G/σ_{Ar} at 100 electron volts. The resulting quantity is the ratio $(\eta A)_G/(\eta A)_{Ar}$. The value 100 electron volts represents an average of the electron energies used by the various RGA's. At this energy, σ is relatively insensitive to small changes in electron energy.

As a rule, the variation (with respect to the test gas) in $(\eta A)_G/(\eta A)_{Ar}$ for any one RGA is considerably less than the variation in s_G/s_{Ar}. This fact suggests that ionization cross section is a major factor in determining sensitivity, although by no means the only factor.

The low values of the ηA ratios listed in table VI for hydrogen and helium for the B-1 RGA could have been increased considerably if the instrument had been tuned for these gases or for others with lower M_s than argon (e.g., M_s = 20 or 28). Davis in reference 35 for a similar 90° sector RGA, also reports a low value of 0.40 for

s_{H_2}/s_{N_2} (principal peak), compared with a value of 0.22 indicated in table IV. Agreement is reasonably close, considering that the accelerating voltage in Davis' test was 1800 volts rather than 4700 volts and that the emission current was 0.1 milliampere rather than 1.0 milliampere.

Value of relative efficiency η_G/η_{Ar}. - The data in table VI for those RGA's using a Faraday cup collector (A = 1), also represent the values of η_G/η_{Ar}. The variation of this quantity with M_s is shown in figure 11. In the range $20 \leq M_s \leq 44$, the values of η_G/η_{Ar} lie within a factor of 2 of being equal to unity for all RGA's.

The variation with M_s is most pronounced for the type A (60° sector) instrument. The relative efficiency appears to vary inversely with M_s. The strong dependence on M_s is believed to result from the fact that scanning voltage also varies inversely with M_s. Therefore, initial ion thermal and dissociation energies contribute more to beam broadening and decreased extraction efficiency β (refs. 17 and 33) at low acceleration energies than at high energies.

Value of overall efficiency η. - The overall efficiency η for argon ions of RGA's with Faraday cup ion collectors can be estimated from the ratio of measured absolute sensitivity (table III) to total argon ion production. The argon ion production can be approximated from known values of σ, l, i^-, p, and T in the ion source. These values of η are listed in the following table for the 60° sector (A1 and A2), the omegatron (D1), and the monopole (F1 and F2) RGA's. In the case of the omegatron, optimum tuning resulted when a portion of the electron current impinged on the electrostatic trap; the ionizing current was taken as the sum of that delivered to the trap and electron collector. The omegatron's high efficiency is largely the result of the low collimated ionizing current (6.5 μA) and the absence of slits to restrict ion collection efficiency. However, cleanliness of the electrode surfaces is particularly important for the proper operation of this instrument (ref. 36).

Instrument	Efficiency, η
A1	0.00016
A2	.0012
D1	.48
F1	.0014
F2	.006

The ratio of efficiencies η for the two ranges of instrument A was 8 to 1 for argon, the accelerating voltage ratio being 6 to 1. In the case of instrument B (with electron multiplier detector), absolute sensitivity (table III) and, therefore, product ηA, were

essentially the same although the accelerating voltage varied 3 to 1 between ranges. The 4 to 1 difference in η for the two ranges of instrument F (see table) is the result of resolution changes (change in U/V_{rf}).

Cracking Patterns

Cracking patterns measured in this investigation are presented in table VII. This table also includes data for the $90^{\circ}/135^{\circ}$ sector instrument (C) located in chamber 3. The cracking patterns published by the ASTM (ref. 37), where available, are also listed, as well as percent natural abundance (PNA) of krypton and xenon isotopes.

These data emphasize the fact that cracking patterns differ widely for different types of RGA's and even differ moderately for different ranges of the same RGA. This is to be expected because of variations in types and operating parameters of ion sources, transmission efficiencies of the different m/q separators, and relative response of electron multiplier detectors, where used, to ions of different m/q and different energies.

The accuracy of the data will depend on RGA resolving power or its ability to measure cross-contribution effects of closely spaced peaks.

The $90^{\circ}/135^{\circ}$ sector instrument and the omegatron have significantly higher subsidiary peaks relative to the parent peak than the other instruments. An unexplained exception is argon for instrument C. This RGA normally operates at a 6-milliampere emission current, compared with 1 or 2 milliamperes for the others. Investigations have shown that relative intensities of parent ions decrease markedly with increasing temperature of the gas, which is assumed to be in thermal equilibrium with ion source surfaces (ref. 38, pp. 202-204).

Where an omegatron has a simple electrode structure, as in the one studied, the rf field is nonuniform, and ions that resonate at a frequency ω_c can also reach the collector at harmonics of ω_c (ref. 39). The high peaks at $1/2\ M_s$ and $1/3\ M_s$ result mainly from this phenomenon rather than from multiple ionization or dissociation. Tuning can minimize this effect, but with a sacrifice of complete mass coverage and performance.

In table VII(b) values for $M_s = 2$ are primarily due to H_2^+ present as a background gas rather than to He^{++}, as the ionization cross section for the latter is negligible for the range of electron energies used (ref. 38, p. 184).

For instrument A the large fraction of triply ionized argon results from the high electron energy (150 V) used, at which the ionization cross section for Ar^{+++} is relatively high (ref. 40). Electron energies for the other RGA's were at or below the threshold value.

The average deviation of relative peak heights among the several runs of the same

gas was about 3 percent, a considerably superior repeatability than that of the absolute sensitivity listed in table III.

Changes in instrument resolution will affect the cracking pattern. Figure 12 shows how the ratio i^+_{14}/i^+_{28} varies with resolution of the quadrupole (in this case tuned for nitrogen).

The cracking pattern for oxygen is hard to define because of the production of carbon monoxide and carbon dioxide from the reaction of incandescent filaments with carbon impurities (ref. 41). Likewise, water ($M_s = 18$) was a reaction byproduct in the oxygen and carbon dioxide cracking patterns. The definition of sensitivity, particularly for oxygen, becomes ambiguous because of these byproducts. The instruments were allowed to stabilize overnight, with a constant flow of oxygen, before the cracking pattern was measured.

Only four instruments were capable of resolving the isotopes of krypton and only two were capable of resolving the isotopes of xenon. For the other instruments the entry in the columnar heading for the singly ionized atom is the sum of all the percentages listed for the PNA. The entry for a multiply ionized atom is in the same proportion to the singly ionized entry as the ratio of measured peak heights.

For some of the instruments with inadequate resolution of krypton or xenon, the inadequacy is due to the fact that the instrument was tuned for argon. Had the instrument been specifically tuned for the particular gas, the isotopes of that gas could have been resolved.

CONCLUSIONS

In order to determine pressures and identities of gases in a vacuum system with a mass spectrometer type of residual gas analyzer (RGA), knowledge of three basic characteristics is required: the absolute sensitivity to a reference gas, the relative sensitivity to other gases, and the cracking pattern of measured gases. This investigation was primarily concerned with determining and comparing these characteristics for 6 such instruments, including magnetic sector, quadrupole, monopole, and omegatron RGA's, and for 10 different gases at a pressure of 2×10^{-7} torr.

Day-to-day variation in absolute sensitivity to argon was about 10 percent, even when voltage and current settings were repeated as closely as the standard control units allowed. Shift in absolute sensitivity after prolonged exposure to oxygen was inconsistent among RGA's, and varied from 30 to 300 percent; some instruments recovered slowly after exposure, and others retained a permanent shift. Absolute gas sensitivity can change considerably for the same RGA when the mass range is changed. The change in s_{Ar} on changing range (by changing electrical or magnetic parameters) varied from 0 to 800 percent for the four RGA's which had multiple ranges.

Overall collection efficiency for the omegatron, as measured, was considerably higher than the others, due to the low electron emission current of 6 microamperes and absence of beam-forming slits or apertures. No single parameter was found that would permit the prediction of an instrument's relative sensitivity for various gases. However, the values of measured relative sensitivity tabulated in this report may be used with an in-place calibration with reference gas such as argon or nitrogen to obtain absolute sensitivity to other gases. A calibration ion gage may be used as a standard in such a calibration with a reference gas.

The accuracy obtainable for relative sensitivity may be judged from the variation in nitrogen-to-argon relative sensitivity obtained over a period of 165 days. It ranges from ± 2 to ± 8 percent for RGA's with Faraday cup detectors to about ± 15 percent for those with electron-multiplier detectors.

The cracking pattern data presented emphasize the fact that cracking patterns differ widely for different types of RGA's and even differ moderately for different ranges of the same RGA. Both sensitivity and cracking pattern depend on the type of RGA, operating parameters of ion sources, transmission efficiencies of the different m/q separators, and relative gain of electron multiplier detectors.

Lewis Research Center,
National Aeronautics and Space Administration,
Cleveland, Ohio, October 3, 1973,
502-04.

APPENDIX - SYMBOLS

A	electron multiplier gain
a	Mathieu equation parameter
a_o	Bohr radius
B	magnetic flux density
D	ion beam dispersion
f	frequency
G	conductance
G_0	leak conductance
G_{12}, G_{23}	orifice conductances
i^-	electron current
i^+	ion current
L	sector RGA distance
L'	monopole RGA distance
ℓ	electron-beam path length
M	atomic mass, amu
M_s	specific atomic mass, samu
ΔM	peak width at 1 percent of peak height, samu
m	ion mass
N_A	Avogadro number
n	molecular density
PNA	percent natural abundance
p	calibration-gas pressure
p_o	calibration-gas pressure, upstream of leak
Q	gas throughput
q	ion charge
q'	Mathieu equation parameter
R	radius of path curvature (sector)
r	radius of quadrupole centers

r_o	radial distance (omegatron)
S	ion gage sensitivity (pressure^{-1})
s	RGA sensitivity (current/pressure
$S\delta$	sensitivity stability
T	temperature
t	time
t_a	flow stabilization time
U	dc voltage amplitude (quadrupole and monopole)
V	ion accelerating voltage, V
V_c	calibration volume
V_d	downstream volume
V_{rf}	voltage amplitude (quadrupole and monopole)
z	(charge of ion)/(charge of electron)
β	ion extraction efficiency
η	ion efficiency, $\beta\tau$
θ	sector angle
ΔM	peak width
σ	total ionization cross section
τ	ion transmission efficiency
ω	angular frequency
ω_c	cyclotron frequency

Subscripts:

1	inlet chamber
2	calibration chamber
3	pump chamber
Ar	argon
G	test gas

REFERENCES

1. Nier, Alfred O.: A Mass Spectrometer for Routine Isotope Abundance Measurement. Rev. Sci. Instr., vol. 11, July, 1940, pp. 212-216.

2. Kiser, Robert W.: Introduction to Mass Spectrometry and Its Applications. Prentice-Hall, Inc., 1965, pp. 22-24.

3. Davis, W. D.; and Vanderslice, L. A.: A Sensitive High-Speed Mass Spectrometer for Ultra-High Vacuum Work. 1960 Transactions of the Seventh National Vacuum Symposium. Pergamon Press, 1961, pp. 417-420.

4. Watson, W. R.; Wallace, R. A.; and Lech, Joseph: Operational Data on the Omegatron as a Vacuum Analyzer. 1960 Transactions of the Seventh National Vacuum Symposium. Pergamon Press, 1961, pp. 421-427.

5. Robinson, Charles F.; and Hall, Laurence G.: Small General Purpose Cycloidal - Focusing Mass Spectrometer. Rev. Sci. Instr., vol. 27, no. 7, July 1956, pp. 504-508.

6. Reich, G.: The Farvitron - A New Partial Pressure Indicator without a Magnetic Field. 1960 Transactions of the Seventh National Vacuum Symposium. Pergamon Press, 1961, pp. 396-400.

7. Bennett, Willard H.: Radiofrequency Mass Spectrometer. J. Appl. Phys., vol. 21, no. 2, Feb. 1950, pp. 143-149.

8. Wiley, W. C.; and McLaren, I. H.: Time-of-Flight Mass Spectrometer with Improved Resolution. Rev. Sci. Instr., vol. 26, no. 12, Dec. 1955, pp. 1150-1157.

9. Paul, W.; Reinhard, H. P.; and Von Zahn, U.: The Electric Mass Filter as a Mass Spectrometer and Isotope Separator. Z. Physik, vol. 152, 1958, pp. 143-182.

10. Brubaker, Wilson M.: The Quadrupole Mass Filter. Presented at the IX Colloquium Spectroscopicum Internationale, Lyon, France, June 1961.

11. von Zahn, Ulf: Monopole Spectrometer, A New Electric Field Mass Spectrometer. Rev. Sci. Instr., vol. 34, no. 1, Jan. 1963, pp. 1-4.

12. Summers, Robert L.: Empirical Observations on the Sensitivity of Hot Cathode Ionization Type Vacuum Gages. NASA TN D-5285, 1969.

13. Holanda, Raymond: Sensitivity of Hot-Cathode Ionization Vacuum Gages in Several Gases. NASA TN D-6815, 1972.

14. Rapp, Donald; and Englander-Golden, Paula: Total Cross Sections for Ionization and Attachment in Gases by Electron Impact. I. Positive Ionization. J. Chem. Phys., vol. 43, no. 5, Sept. 1, 1965, pp. 1464-1479.

15. Chantreau, J.; and Vauthier, R.: Influence of Ion Initial Energies on the Discrimination in a Nier Ion Source Operating without an Auxiliary Magnetic Field and Neglecting the Space-Charge Effect. Recent Developments in Mass Spectroscopy. Koreichi Ogata and Terus Hayakawa, ed., University Park Press, 1970, pp. 198-204.

16. Berry, Clifford E.: Effects of Initial Energies on Mass Spectra. Phys. Rev., vol. 78, no. 5, June 1, 1950, pp. 597-605.

17. Werner, H. W.; Venema, A.; and Linssen, A. J.: Design of a Small Magnetic - Sector Mass Spectrometer with Reduced Mass Discrimination. J. Vac. Sci. Tech., vol. 9, no. 1, Jan.-Feb. 1972, pp. 216-218.

18. Anon.: Source Characteristics of the MS10. Tech. Information Sheet 110, Technical Information Vol. 1, Associated Electric Industries, Ltd., 1969, pp. 11-18.

19. Bailey, J. R.: Residual Gas Spectra in High and Very High Vacuum Systems. Supp. Al Nuovo Cimento, vol. 1, no. 2, 1963, pp. 494-519.

20. Hultzman, William W.: Characteristics, Selection, and Use of Residual Gas Analyzers. NASA TM X-1281, 1966.

21. Nicollian, Edward H.: A Laboratory Leak Detector Using an Omegatron. 1960 Transactions of the Seventh National Vacuum Symposium. Pergamon Press, 1961, pp. 80-86.

22. Sommer, H.; Thomas, H. A.; and Hipple, J. A.: The Measurement of e/M by Cyclotron Resonance. Phys. Rev., vol. 82, no. 5, 1951, pp. 697-702.

23. Dawson, P. H.: Fringing Fields in the Quadrupole Mass Filter. Int. J. Mass Spectrom. Ion Phys., vol. 6, 1971, pp. 33-44.

24. Woodward, C. E.; and Crawford, C. K.: Design of a Quadrupole Mass Spectrometer. Tech. Rep. 176, Lab. for Insulation Research, Massachusetts Inst. Tech., Jan. 1963.

25. Brubaker, Wilson M.; and Tuul, Johannes: Performance Studies of a Quadrupole Mass Filter. Rev. Sci. Instr., vol. 35, no. 8, Aug. 1964, pp. 1007-1010.

26. van Gorkom, M.; and Glick, R. E.: Electron Multiplier Response Under Positive Ion Impact. I. Secondary Electron Emission Coefficients. Int. J. Mass Spectrom. Ion. Phys., vol. 4, 1970, pp. 203-218.

27. Collins, R. D.: The Use of Electron Multipliers in Mass Spectrometry. Vacuum, vol. 19, no. 3, Mar. 1969, pp. 105-111.

28. Normand, C. E.: Use of a Standard Orifice in the Calibration of Vacuum Gauges. 1961 Transactions of the Eighth National Vacuum Symposium. Vol. 1, Pergamon Press, 1962, pp. 534-543.

29. Owens, Charles L.: Ionization Gauge Calibration System Using a Porous Plug and Orifice. J. Vac. Sci. Tech., vol. 2, no. 3, May/June 1965, pp. 104-108.

30. Santeler, Donald J.; Holkeboer, David H.; Jones, Donald W.; and Pagano, Frank: Vacuum Technology and Space Simulation. NASA SP-105, 1966, pp. 83-121.

31. Bureau, A. J.; Laslett, L. Jackson; and Keller, J. M.: The Pumping Speed of a Circular Aperture in a Diaphragm Across a Circular Tube. Rev. Sci. Instr. vol. 23, no. 12, Dec. 1952, pp. 683-686.

32. Holanda, Raymond: Evaluation of a Volume-Ratio System for Vacuum Gage Calibration from 10^{-8} to 10 Torr. NASA TN D-5406, 1969.

33. Coggeshall, Norman D.: Discrimination in Mass Spectrometer Ion Sources. J. Chem. Phys., vol. 12, no. 1, Jan. 1944, pp. 19-23.

34. Brunnée, C.; Delgmann, L.; and Kronenberger, K.: The Atlas Quadrupole Mass Spectrometer. Presented at the Eleventh Annual Conference on Mass Spectrometry and Allied Topics (ASTM Comm. E-14), San Francisco, Calif., 1963.

35. Davis, William D.: Ultra-high Vacuum Gauge Calibration. J. Vac. Sci. Tech., vol. 5, no. 1, Jan.-Feb. 1968, pp. 23-33.

36. Pytkowski, S.; and Szwemin, P.: The Stability of Omegatron Sensitivity for Different Electrode Materials. Advances in Vacuum Science and Technology. Vol. 2, part 2. H. Adam, ed., Pergamon Press, 1967, pp. 505-507.

37. ASTM Comm. E-14 on Mass Spectrometry: Index of Mass Spectral Data. Spec. Tech. Publ. No. 356, ASTM, 1963.

38. Field, F. H.; and Franklin, J. L.: Electron Impact Phenomena and the Properties of Gaseous Ions. Second ed., Academic Press, 1970, pp. 202-204.

39. Bijma, J.; Suurmeijer, E. P. Th. M.; and Francken, J. C.: Properties of Omegatrons with Non-unifrom R. F. Fields. Proceedings of the Fourth International Vacuum Congress. Part 2. Adlard and Son, Ltd., 1968, pp. 729-733.

40. Bleakney, Walter: Ionization Potentials and Probabilities for the Formation of Multiply Charged Ions in Helium, Neon, and Argon. Phys. Rev., vol. 36, Oct. 1930, pp. 1303-1308.

41. Singleton, J. H.: Interaction of Oxygen with Hot Tungsten. J. Chem. Phys., vol. 45, no. 8, Oct. 15, 1966, pp. 2819-2826.

TABLE I. - TOTAL IONIZATION

CROSS SECTION

Gas	Total ionization cross section, σ, at -		
	[a]75 eV	[a]100 eV	[a]150 eV
Hydrogen	1.103	1.050	0.924
Helium	.380	.416	.419
Neon	.622	.758	.878
Nitrogen	2.72	2.87	2.79
Carbon monoxide	2.88	3.01	2.92
Oxygen	2.80	3.04	3.06
Argon	3.20	3.24	3.05
Carbon dioxide	3.72	4.00	3.96
Krypton	4.83	4.77	4.35
Xenon	5.84	6.12	5.90

[a]Multiples of πa_o^2 (where $\pi a_o^2 = 87.94 \times 10^{-18}$ cm^2).

TABLE II. - RESIDUAL GAS ANALYZER CHARACTERISTICS

Instrument designation	Range designation	Type of instrument	Range of specific atomic mass, M_s, samu	M_s-scan means	Range change means	Accelerating voltage, V	Magnetic flux T	Electron energy, eV	Electron emission, mA	Filament material	Dynode material
A	A1	60° sector	2 - 44	V	Magnet shunt	100 - 2000	0.45	150	1	Tungsten	----------
	A2[d]	60° sector	10 - 300	V	Magnet shunt	100 - 2000	.18	150	1	Tungsten	----------
B	B1[d]	90° sector[b]	2 - 200	V	Magnet current	75 - 4700	.28	75	1	Tungsten	Silver-magnesium
	B2	90° sector[b]	1 - 90[a]	B	V	750	0.01 - 0.07	75	1	Tungsten	Silver-magnesium
C	C1[d]	90° sector[c]	10 - 80+	V	Sector angle	60 - 500	0.15	86	6	Tungsten	----------
	C2	135° sector[c]	1 - 10	V	Sector angle	50 - 1000	.15	86	6	Tungsten	----------
D	D1	Omegatron	1 - 50	f	----------	0 - 1	0.4	75	0.006	Tungsten	----------
E	E1[d]	Quadrupole[b]	1 - 50	V	f	15	----------	90	1	Tungsten	Copper-beryllium
	E2	Quadrupole[b]	1 - 150	V	f	15	----------	90	1	Tungsten	Copper-beryllium
F	F1[d]	Monopole	1 - 50	V	Ratio of U/V	15 - 30	----------	85	2	Tungsten-rhenium	----------
	F2	Monopole	1 - 200	V	Ratio of U/V	15 - 30	----------	85	2	Tungsten-rhenium	----------

[a] 1 to 150 with 500 V accelerating voltage.

[b] With electron multiplier detector.

[c] Only cracking patterns were studied.

[d] Instrument tuned on this range for maximum sensitivity to Ar.

TABLE III. - MEAN ABSOLUTE SENSITIVITY TO ARGON-40 AND AVERAGE DEVIATION FROM MEAN, BEFORE EXPOSURE TO OXYGEN

RGA designation	Range designation	Range of specific atomic mass, M_s, samu	Average absolute sensitivity, s_{Ar}, A/torr	Average deviation, percent
A	A1	2 - 44	4.3×10^{-6}	13
	A2	10 - 300	34×10^{-6}	12
B	B1	2 - 200	0.055	12
	B2	1 - 90	.050	19
D	D1	1 - 50	34×10^{-6}	7
E	E1	1 - 50	2.0	13
	E2	1 - 150	.60	15
F[a]	F1	1 - 50	26×10^{-6}	12
	F2	1 - 200	112×10^{-6}	7

[a]Runs 10 to 20 only.

TABLE IV. - SENSITIVITY RELATIVE TO ARGON. PRINCIPAL-PEAK RATIOS

Gas	Parent peak, M_s, samu	Instrument range designation								
		A1	A 2	B1	B2	D1	E1	E2	F1	F2
		Sensitivity to argon, s_G/s_{Ar}								
Hydrogen	2	12.8	----	0.25	1.85	0.16	0.21	0.30	0.76	0.18
Helium	4	5.4	----	.082	.120	.084	.106	.063	.49	.122
Neon	10	.42	0.43	.32	.28	.13	.128	.117	.25	.150
Nitrogen	28	.91	1.00	1.14	1.12	.70	.88	.83	.79	.55
Carbon monoxide	28	1.19	1.05	1.52	1.41	.72	1.12	.94	.90	.60
Oxygen	32	.84	.68	.93	1.02	.46	.82	.78	.44	.38
Argon	40	1.00	1.00	1.00	1.00	1.00	1.00	1.00	1.00	1.00
Carbon dioxide	44	.93	.80	1.14	1.18	.88	1.48	1.39	.61	.80
Krypton	84	----	.24	.111	.39	----	----	.96	----	1.06
Xenon	132	----	.12	.096	.095	----	----	.92	----	1.9

TABLE V. - SENSITIVITY RELATIVE TO ARGON. RATIO OF SUM OF PEAKS

Gas	Sum of peaks, M_s	Instrument range designation								
		A1	A2	B1	B2	D1	E1	E2	F1	F2
		Sensitivity to argon, s_G/s_{Ar}								
Hydrogen	2	8.4	----	0.22	----	-----	-----	-----	----	-----
Hydrogen	2 + 1	----	----	-----	1.61	0.101	0.20	0.28	0.61	0.16
Helium	4 + 2	3.6	----	.075	.104	.053	.099	.059	.39	.111
Neon	20 + 10 + 11 + 21 + 22	.35	0.37	.30	.26	.14	.131	.122	.24	.140
Nitrogen	28 + 14 + 15 + 29	.70	.88	1.10	1.08	.74	.86	.82	.74	.54
Carbon monoxide	28 + 12 + 14 + 16 + 29 + 30	.87	.90	1.42	1.31	.76	1.09	.91	.79	.57
Oxygen	32 + 16	.69	.60	.95	1.11	.50	.85	.82	.50	.48
Oxygen	32 + 12 + 14 + 16 + 18 + 22 + 28 + 44	.82	.72	1.03	1.23	.68	1.03	1.01	.61	.49
Argon	$40 + 13\frac{1}{3} + 20 + 36 + 38$	1.00	1.00	1.00	1.00	1.00	1.00	1.00	1.00	1.00
Carbon dioxide	44 + 12 + 16 + 18 + 22 + 28 + 32	.98	.88	1.65	1.77	1.14	1.66	1.56	.87	.90
Krypton	84 + 78 + 80 + 82 + 83 + 86 + (~40)	----	.62	.37	.95	-----	-----	2.33	----	2.46
Xenon	132 + 124 + 126 + 128 + 129 + 130 + 131	----	.64	.45	.45	-----	-----	3.68	----	7.56
	+ 134 + 136 + (~33 + ~44 + ~66)	----	----	-----	-----	-----	-----	-----	----	----

TABLE VI. - VALUE OF $(\eta A)_G/(\eta A)_{Ar}$

Gas	Instrument range designation								
	A1	A2	B1	B2	D1	E1	E2	F1	F2
	$(\eta A)_G/(\eta A)_{Ar}$								
Hydrogen	26	----	0.68	4.9	0.31	0.62	0.87	1.89	0.50
Helium	28	----	.58	.81	.41	.77	.46	3.0	.86
Neon	1.50	1.58	1.28	1.11	.60	.56	.52	1.03	.60
Nitrogen	.79	.99	1.23	1.22	.84	.97	.93	.84	.61
Carbon monoxide	.94	.97	1.53	1.41	.82	1.17	.98	.85	.61
Oxygen	.74	.64	1.01	1.18	.53	.91	.87	.53	.53
Carbon dioxide	.79	.71	1.34	1.43	.92	1.34	1.26	.70	.73
Krypton	-----	.42	.25	.65	----	----	1.58	----	2.61
Xenon	-----	.34	.24	.24	----	----	1.95	----	4.00

TABLE VII. - CRACKING PATTERNS FOR VARIOUS GASES

(a) Hydrogen

Instrument range designation	Specific atomic mass, M_s, samu		Total
	1	2	
	Cracking pattern, percent of principal peak		
A1	----	100	100
B1	----	↓	100
B2	0.74		101
C2	5.0		105
D1	.92		101
E1	1.49		101
E2	----		100
F1	1.40		101
F2	----		100
ASTM	2	↓	102

(b) Helium

Instrument range designation	Specific atomic mass, M_s, samu		Total
	2	4	
	Cracking pattern, percent of principal peak		
A1	1.50	100	102
B1	5.4	↓	105
B2	1.27		101
C2	3.75		104
D1	1.14		101
E1	1.38		101
E2	1.01		101
F1	1.29		101
F2	1.70		102
ASTM	----	---	---

(c) Neon

Instrument range designation	Specific atomic mass, M_s, samu					Total
	10	11	20	21	22	
	Cracking pattern, percent of principal peak					
A1	17.4	1.55	100	0.42	9.0	128
A2	-----	-----	↓	.30	9.9	110
B1	-----	-----		.30	9.2	109
B2	.04	-----		.26	9.2	109
C1	-----	-----		----	55	155
D1	52	2.09		----	15.7	170
E1	.95	.11		.29	9.7	111
E2	1.20	.12		.34	9.8	112
F1	10.1	-----		----	9.7	120
F2	3.90	-----		----	----	104
ASTM	<1	<1	↓	1	10	111

TABLE VII. - Continued. CRACKING PATTERNS FOR VARIOUS GASES

(d) Nitrogen

Instrument range designation	Specific atomic mass, M_s, samu				Total
	14	15	28	29	
	Cracking pattern, percent of principal peak				
A1	16.0	-----	100	0.73	117
A2	11.7	0.05		.70	112
B1	10.1	-----		.57	111
B2	11.0	-----		.58	112
C1	24.1	-----		----	124
D1	69	-----		----	169
E1	6.7	.03		.67	107
E2	6.0	.03		.62	107
F1	17.8	1.56		----	119
F2	9.5	-----		----	110
ASTM	5	<1		1	106

(e) Carbon monoxide

Instrument range designation	Specific atomic mass, M_s, samu						Total
	12	14	16	28	29	30	
	Cracking pattern, percent of principal peak						
A1	6.1	2.53	1.08	100	1.10	----	111
A2	4.7	1.63	1.79		1.12	0.15	109
B1	5.2	.57	1.20		1.06	----	108
B2	5.2	.77	1.15		1.18	.18	108
C1	22.2	6.5	----		----	----	128
D1	5.6	60	3.78		----	----	169
E1	3.19	.38	1.63		1.03	.19	106
E2	2.18	.30	1.44		1.02	.17	105
F1	6.44	.85	2.53		----	----	110
F2	3.52	-----	2.93		----	----	106
ASTM	5	1	2		1	1	110

TABLE VII. - Continued. CRACKING PATTERNS

FOR VARIOUS GASES

(f) Oxygen

Instrument range designation	Specific atomic mass, M_S, samu								Total
	12	14	16	18	22	28	32	44	
	Cracking pattern, percent of principal peak								
A1	1.81	----	24.9	6.9	----	9.5	100	6.0	149
A2	1.12	0.13	12.2	2.94	0.87	8.2	↓	9.3	135
B1	1.17	.07	16.5	1.50	.14	4.8		4.5	129
B2	1.64	----	26.3	2.27	.22	4.8		5.1	140
C1	6.8	----	51	11.7	----	20.4		17.9	207
D1	.24	2.17	73	1.71	6.7	44		7.2	235
E1	.61	.04	12.7	1.37	.22	6.9		14.7	137
E2	.50	.08	13.5	1.34	.10	7.3		16.0	139
F1	3.43	----	42	4.0	----	12.9		10.9	173
F2	-----	----	27.2	-----	----	----		18.8	146
ASTM	<1	----	5	-----	----	3	↓	<1	108

(g) Argon

Instrument range designation	Specific atomic mass, M_S, samu					Total
	$13\frac{1}{3}$	20	36	38	40	
	Cracking pattern, percent of principal peak					
A1	4.1	48	----	-----	100	152
A2	1.3	26	0.4	0.07	↓	127
B1	0	16	----	-----		116
B2	0	16	----	-----		116
C1	0	7	----	-----		107
D1	2	60	----	-----		162
E1	0	8.4	.4	0		109
E2	↓	7.4	.3	0		108
F1		25	----	-----		125
F2		12	----	-----		112
ASTM	<1	13	<1	<1	↓	114

TABLE VII. - Continued. CRACKING PATTERNS FOR VARIOUS GASES

(h) Carbon dioxide

Instrument range designation	Specific atomic mass, M_s, samu							Total
	12	16	18	22	28	32	44	
	Cracking pattern, percent of principal peak							
A1	11	22	0	5	21	0	100	159
A2	5	10	.3	4	21	.08	↓	141
B1	20	23	.6	1.5	22	.4	↓	167
B2	24	26	.6	1.3	22	.3	↓	174
C1	29	33	0	0	39	0	↓	201
D1	5	8	5.6	66	12	10	↓	207
E1	3.0	4.8	.2	.8	13	.1	↓	122
E2	3.6	4.1	.1	.7	13	.1	↓	121
F1	20	24	0	3.6	31	0	↓	179
F2	5	7	0	0	14	----	↓	126
ASTM	5	7	0	1.5	7	1	↓	121

(i) Krypton

Instrument range designation	Specific atomic mass, M_s, samu								Total
	39 - 43	78	80	82	83	84	86	[a]78 - 86	
	Cracking pattern, percent of principal peak								
A2	162	0.60	4.3	19.5	19.7	100	28.9	---	335
B1	209	.71	4.3	20.8	20.3	100	27.2	---	382
B2	106	.69	4.2	21.0	21.8	100	30.4	---	284
C1	[b]703	----	----	----	----	---	----	176	879
E2	90	.68	3.45	19.5	19.9	100	31.3	---	265
F2	[b]84	----	----	----	----	---	----	176	260
PNA	----	.62	4.0	20.3	20.3	100	30.5	---	176

[a]Sum of Kr^+ isotopes M_s 78 to 86 based on PNA (M_s 84 = 100 percent).
[b]Sum of Kr^{++} isotopes as percent of (a), based on peak current readings.

TABLE VII. - Concluded. CRACKING PATTERNS FOR VARIOUS GASES

(j) Xenon

Instrument range designation	Specific atomic mass, M_s, samu													Total
	31 - 34	41.3 - 45.3	62 - 68	124	126	128	129	130	131	132	134	136	[a]124-136	
	Cracking pattern, percent of principal peak													
A-2	[b]16	[b]168	[b]168	0.35	0.29	-----	79.4	-----	73.5	100	35	29	---	669
B-1	---	[c]15	[c]156	------	------	-----	-----	-----	----	---	--	--	372	543
B-2	---	[c]15	[c]167	------	------	-----	-----	-----	----	---	--	--	372	554
E-2	---	[b]6	[b]49	.46	.46	10	100	18.6	82.1	100	35	29	---	430
F-2	---	----	[c]74	------	------	-----	-----	-----	----	---	--	--	372	446
ASTM	---	----	[d]18	<18	<18	<18	98	<18	79	100	38	32	---	---
PNA	---	----	----	.28	.33	7.1	98.3	15.2	78.8	100	38	33	---	372

[a]Sum of Xe^+ isotopes M_s 124 to 136 based on PNA (M_s 132 = 100%)

[b]Sum of Xe^{++} and Xe^{+++} isotopes as percent of measured sum of all Xe^+ isotopes.

[c]Same as (b), but based on peak meter readings.

[d]For M_s = 66.

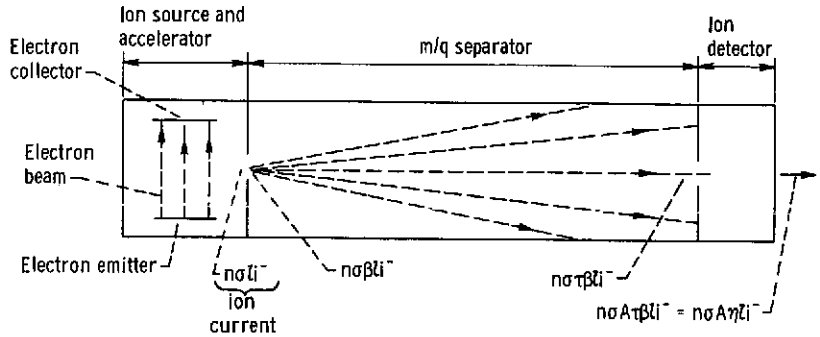

Figure 1. - Basic elements of a residual gas analyzer.

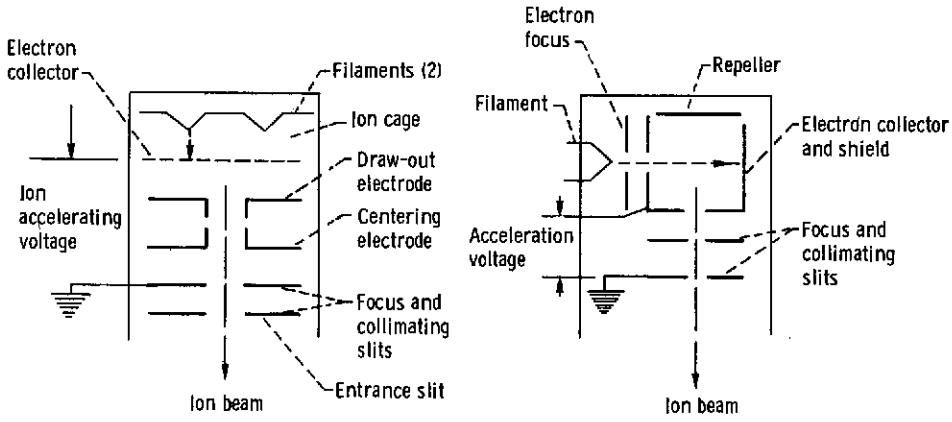

(a) Parallel electron and ion beams.

(b) Perpendicular electron and ion beams.

Figure 2. - Ion sources and accelerators.

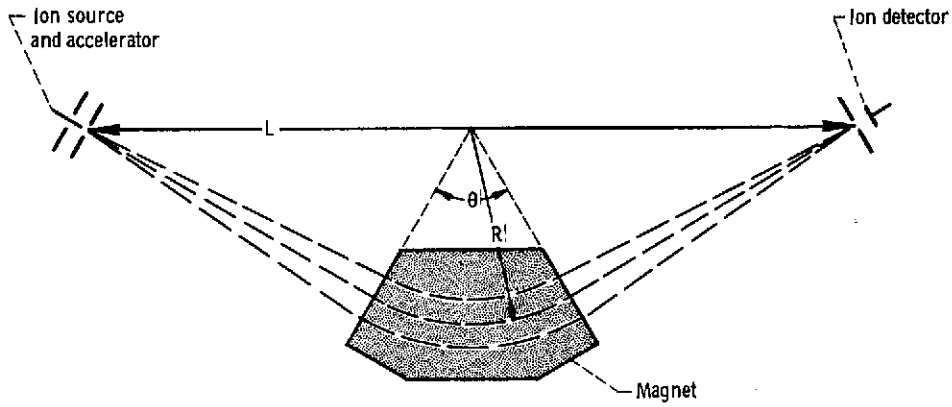

(a) Sector.

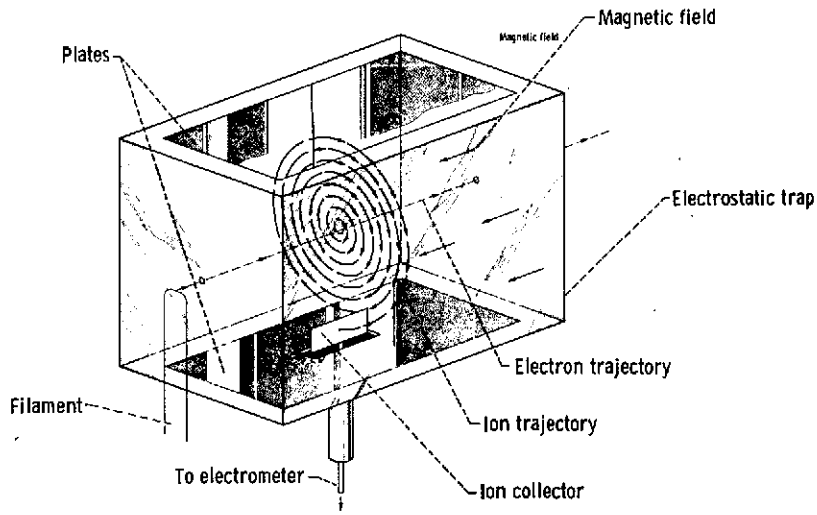

(b) Omegatron.

Figure 3. - Mass-to-charge-ratio separators, sector and omegatron types.

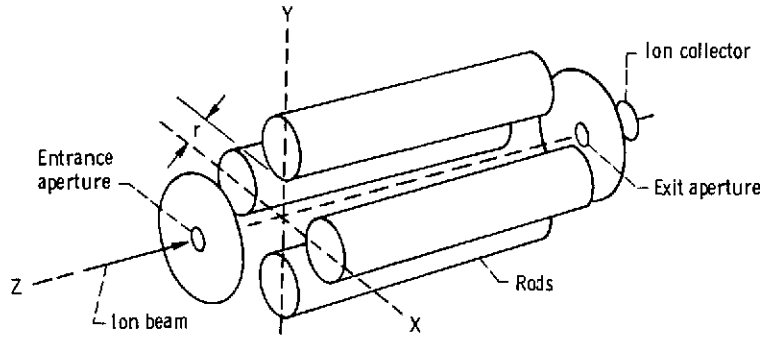

(a) Quadrupole.

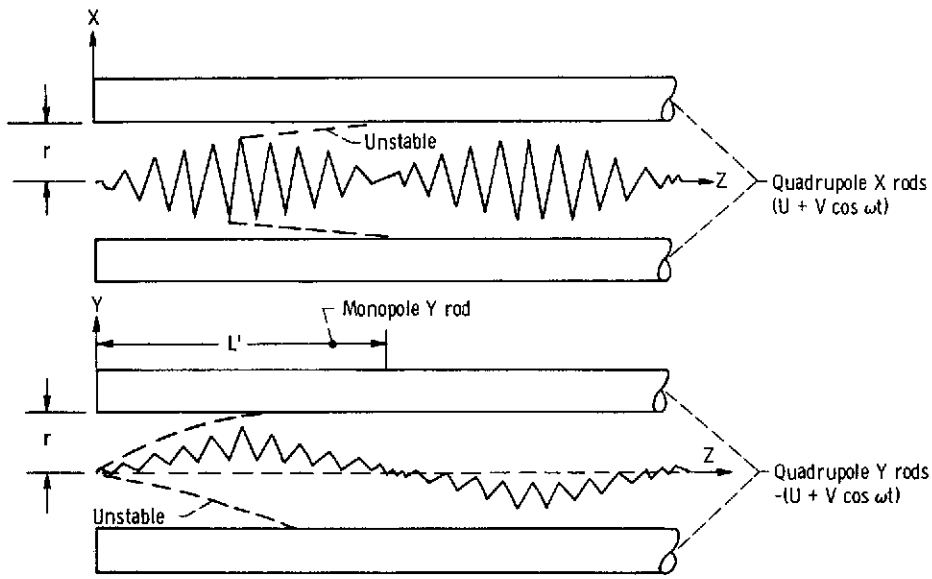

(b) Ion trajectories.

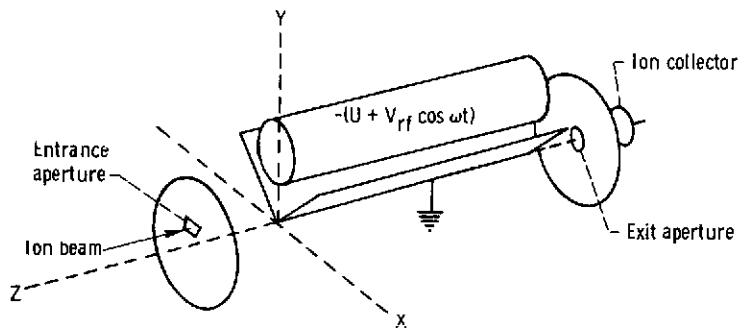

(c) Monopole.

Figure 4. - Mass-to-charge-ratio separator, quadrupole and monopole types.

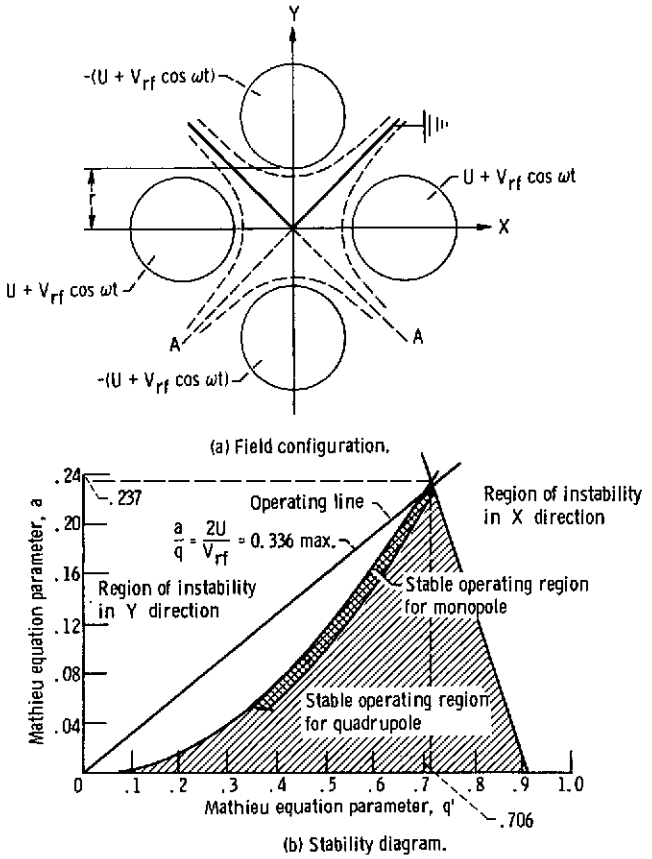

Figure 5. - Field configuration and stability diagram for quadrupole and monopole RGA's.

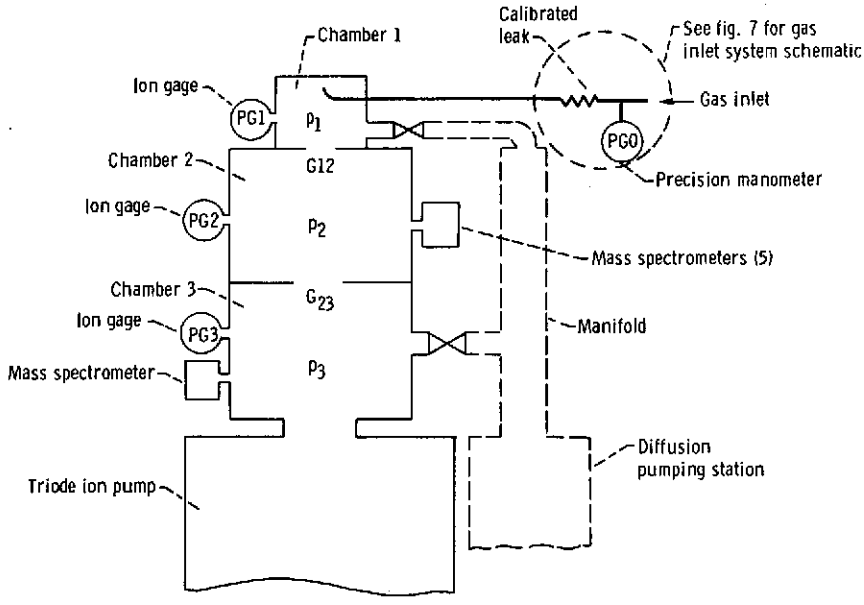

Figure 6. - Mass spectrometer calibration apparatus.

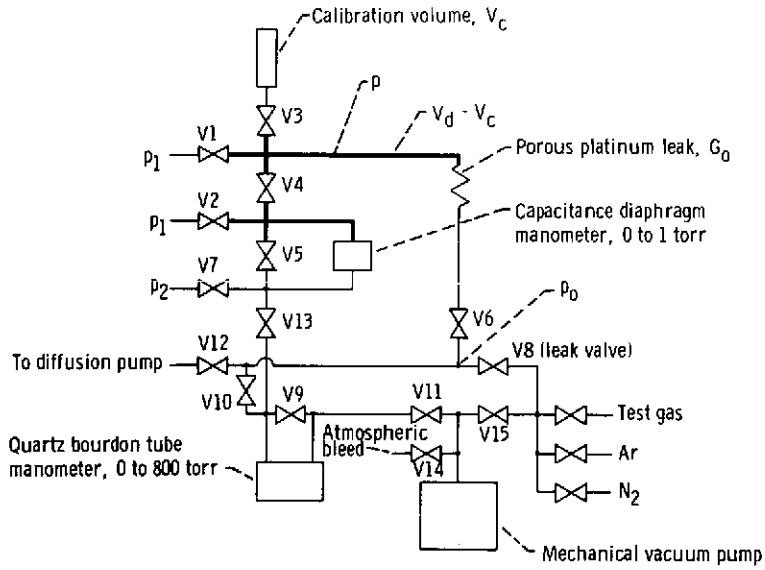

Figure 7. - Gas inlet and leak calibration apparatus.

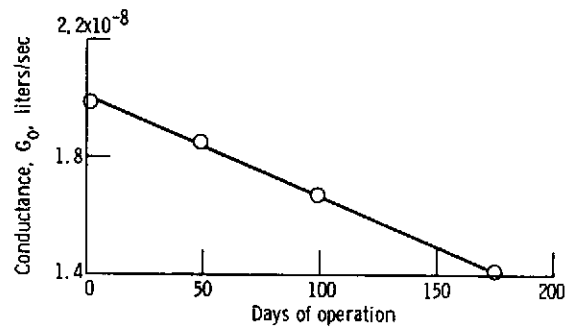

Figure 8. - Drift of conductance of porous platinum leak.

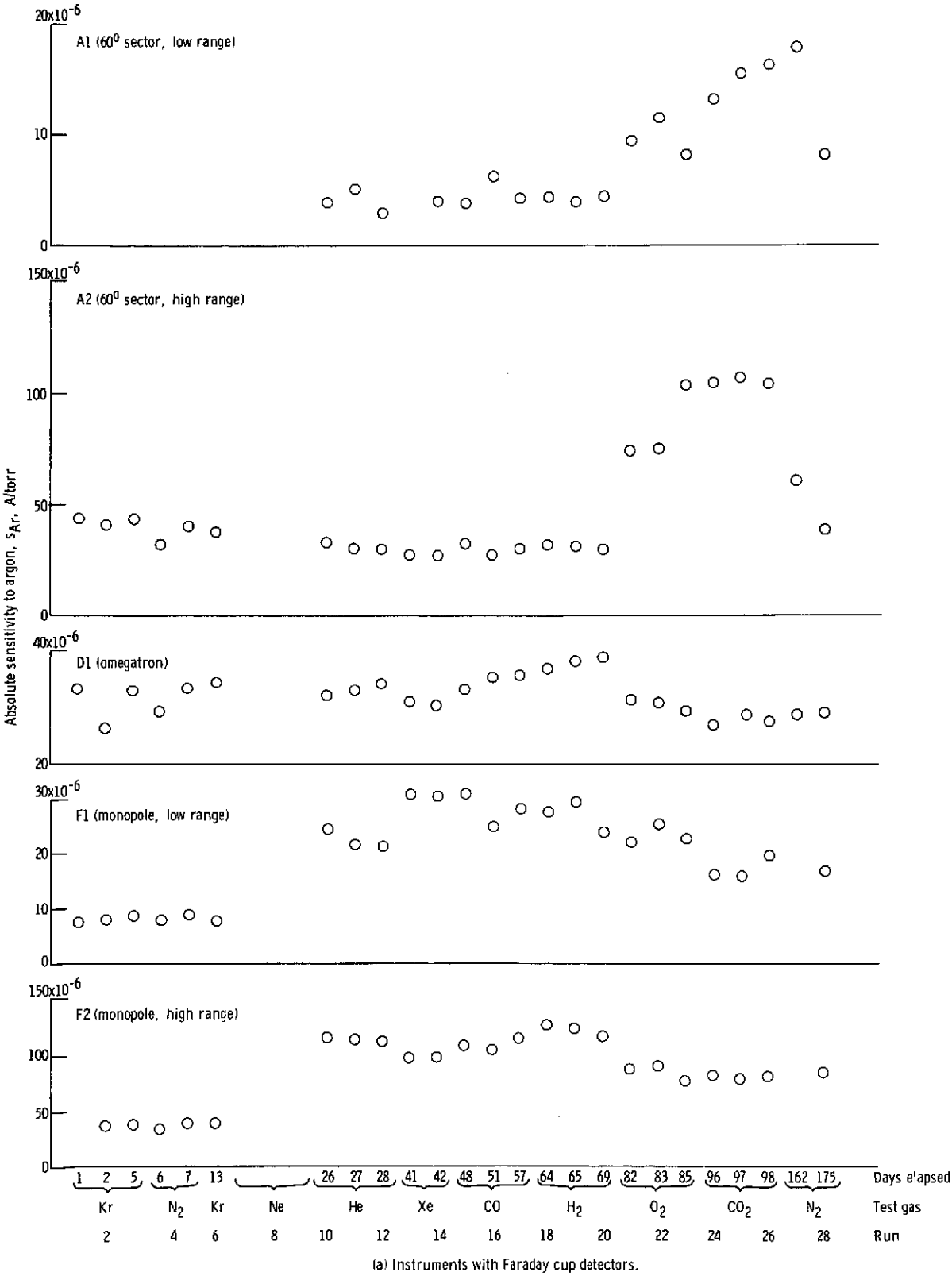

(a) Instruments with Faraday cup detectors.

^ - Chronological history of sensitivity to argon. Test gas calibration preceded argon calibration on same date.

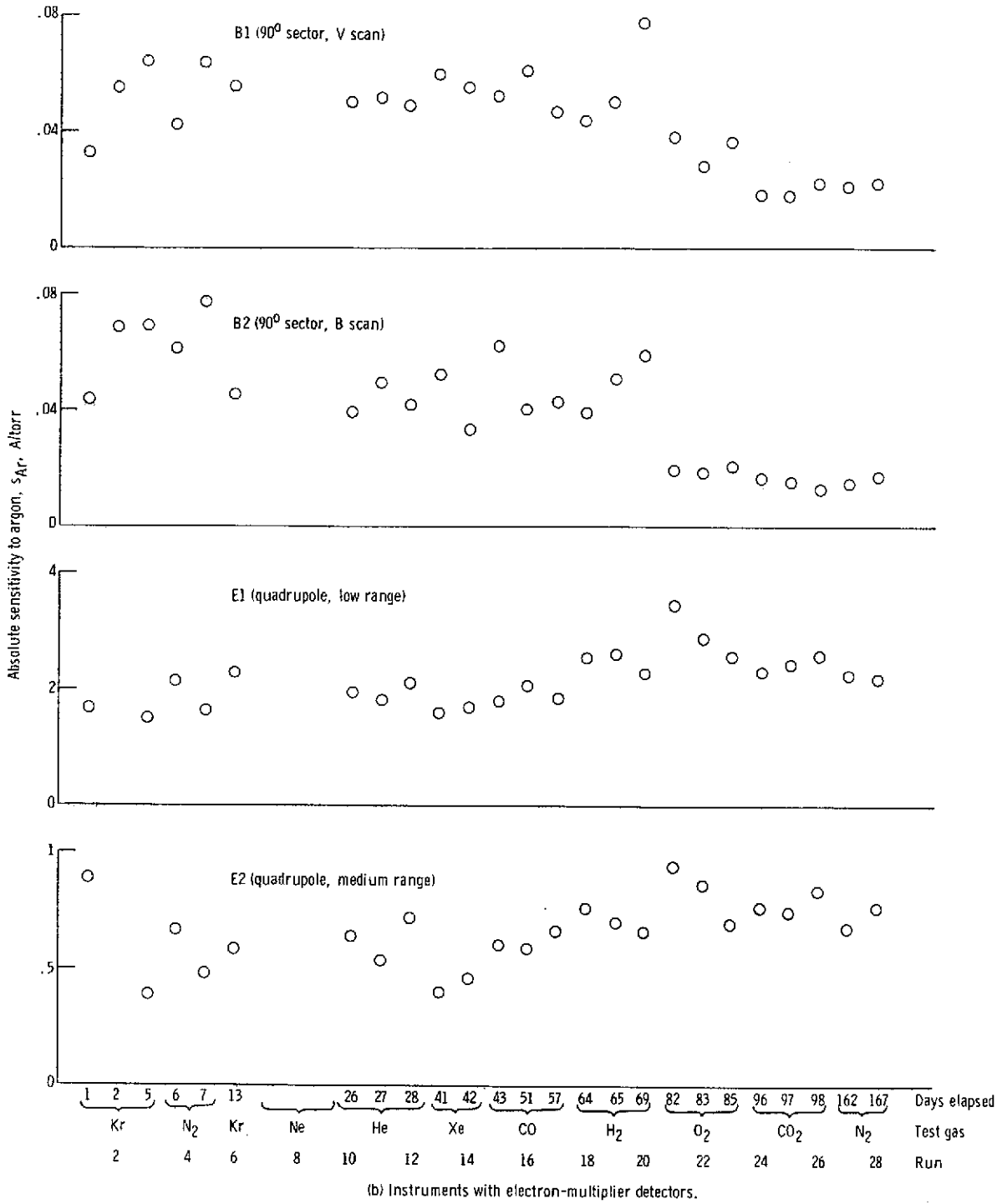

(b) Instruments with electron-multiplier detectors.

Figure 9. - Concluded.

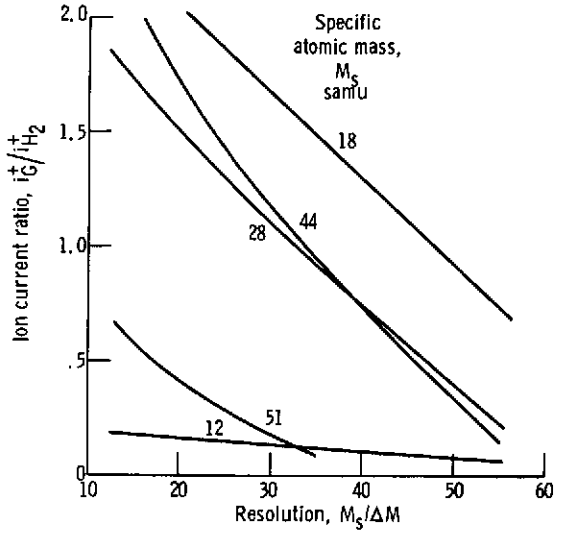

Figure 10. - Effect of resolution on apparent background of vacuum system as indicated by E1 quadrupole RGA. Total equivalent nitrogen pressure was 2.4×10^{-9} torr.

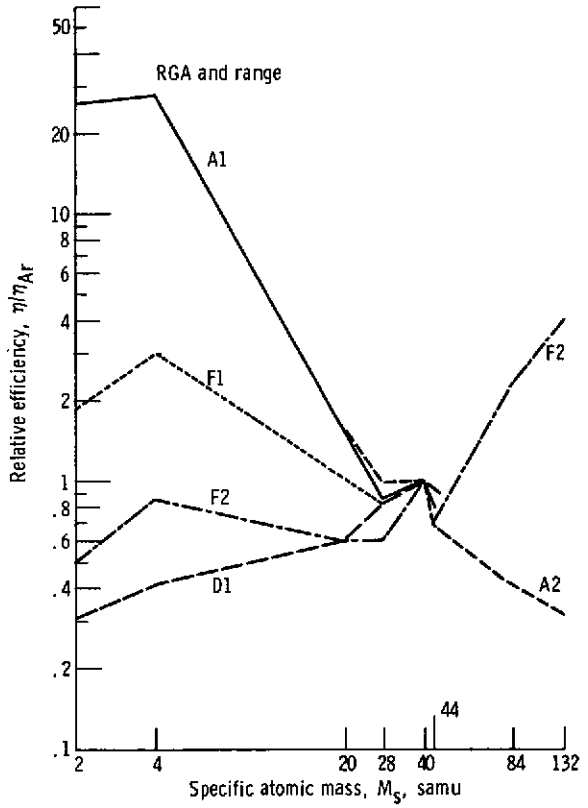

Figure 11. - Variation of relative efficiency with specific atomic mass for RGA's using a Faraday cup collector (A = 1).

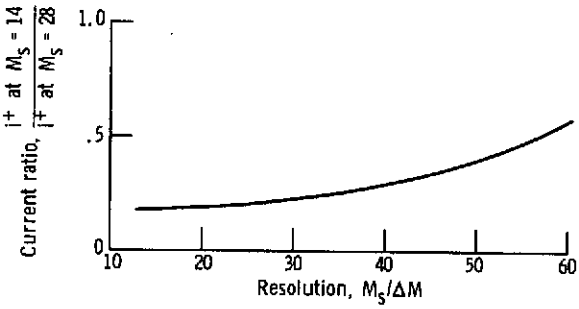

Figure 12. - Effect of resolution on nitrogen cracking pattern of E1 quadrupole RGA.

NASA-Langley, 1974 E-7432